# Triad interaction stabilizes the voltage sensor domains in a constitutively open KCNQ1-KCNE3 channel

Go Kasuya[1], Koichi Nakajo[1]*

[1]*Division of Integrative Physiology, Department of Physiology, Jichi Medical University, 3311-1 Yakushiji, Shimotsuke, Tochigi, Japan 320-0498*

* Correspondence and requests for materials should be addressed to K.N. (knakajo@jichi.ac.jp)

## Abstract

Tetrameric voltage-gated $K^+$ channels have four identical voltage sensor domains, and they regulate channel gating. KCNQ1 (Kv7.1) is a voltage-gated $K^+$ channel, and its auxiliary subunit KCNE proteins dramatically regulate its gating. For example, KCNE3 makes KCNQ1 a constitutively open channel by affecting the voltage sensor movement. However, how KCNE proteins regulate the voltage sensor domain is largely unknown. In this study, by utilizing the recently determined KCNQ1-KCNE3-calmodulin complex structure, we identified amino acid residues on KCNE3 facing the S1 segment of KCNQ1 that are required for constitutive activity. In addition, we found that the interaction of these amino acid residues of KCNE3 and the S1 segment affects the voltage sensor movement via M238 and V241 residues of the S4 segment. This triad interaction shifts the voltage sensor domain's equilibrium, leading to stabilization of the channel's open state.

## Introduction

KCNQ1 (Kv7.1) is a voltage-gated $K^+$ channel. Its gating behavior depends mainly on its auxiliary subunit KCNE proteins (Wang et al., 2020). There are five KCNE genes in the human genome, and all of them are known to modify KCNQ1 channel gating behavior, at least in *Xenopus* oocytes or mammalian cell lines (Bendahhou et al., 2005). Therefore, the physiological functions of the KCNQ1 channel are determined by the type of KCNE proteins that are co-expressed in a tissue. The most well-known example is the cardiac KCNQ1-KCNE1 channel, which underlies the slow cardiac delayed-rectifier $K^+$ current ($I_{Ks}$) (Barhanin et al., 1996; Sanguinetti et al., 1996; Takumi et al., 1988). Another example is the KCNQ1-KCNE3 channel, a constitutively open channel expressed in epithelial cells in the trachea, stomach, and intestine. This channel complex couples with some ion transporters to facilitate ion transport by recycling $K^+$ ions (Abbott, 2016; Grahammer et al., 2001; Preston et al., 2010; Schroeder et al., 2000). The mechanisms by which KCNE proteins modify KCNQ1 channel gating behavior have been a central question of this ion channel. Since KCNQ1 is a classic shaker-type tetrameric voltage-gated $K^+$ channel, it has four independent voltage-sensing domains (VSDs), one from each α subunit (Long et al., 2005). Each VSD consists of four transmembrane segments, S1-S4. Each S4 segment bears several positively-charged amino acid residues. When the membrane potential is depolarized, each S4 segment moves upward (towards the extracellular side). That upward movement eventually triggers pore opening (Jensen et al., 2012; Larsson et al., 1996; Mannuzzu et al., 1996). Therefore, the S4 segment is considered to be an essential part of voltage-sensing (Aggarwal and MacKinnon, 1996; Catterall, 1988; Fedida and Hesketh, 2001; Liman and Hess, 1991; Logothetis et al., 1992; Noda et al., 1984; Papazian et al., 1991). As in the *Shaker* $K^+$ channel, the S4 segment of the KCNQ1 channel also moves upward with depolarization, as proved by scanning cysteine accessibility mutagenesis (SCAM) (Nakajo and Kubo, 2007; Rocheleau and Kobertz, 2008) and voltage-clamp fluorometry (VCF) (Barro-Soria et al.,

2014; Nakajo and Kubo, 2014; Osteen et al., 2012, 2010). In those studies, the presence of KCNE proteins was found to affect the voltage sensor movement. These results suggest that each type of KCNE protein stabilizes a specific state during the voltage sensor transition (Barro-Soria et al., 2017, 2015, 2014; Nakajo, 2019). There should be at least three positions in the VSDs of KCNQ1: “down”, “intermediate”, and “up” (Hou et al., 2017; Taylor et al., 2020). KCNE1 stabilizes the intermediate position of VSDs along with a direct interaction of the pore domain. In contrast, KCNE3 may stabilize the intermediate or up position of VSDs and indirectly stabilize the channel's open state (Barro-Soria et al., 2017, 2015; Taylor et al., 2020).

Early studies by Melman *et al.* revealed “the triplet” of amino acid residues in the middle of the transmembrane segment (“FTL” in KCNE1 and “TVG” in KCNE3) as structural determinants of KCNE modulation properties (Melman et al., 2002, 2001). Exchanging the triplet (or one of the three amino acid residues) between KCNE1 and KCNE3 could introduce the other’s modulation properties, at least partially. For example, introducing “FTL” into KCNE3 transforms it into a KCNE1-like protein. Therefore, it has been long considered that “the triplet” is a functional interaction site between KCNQ1 and KCNE proteins. Possible interaction sites of the KCNQ1 side have also been explored and are believed to be located between the pore domain and the VSD (Chung et al., 2009; Kang et al., 2008; Nakajo and Kubo, 2007; Van Horn et al., 2011; Xu et al., 2008). By utilizing the KCNQ1 ortholog from ascidian *Ciona intestinalis*, which lacks KCNE genes, we previously found that F127 and F130 of the S1 segment are required for KCNE3 to make KCNQ1 a constitutively open channel (Nakajo et al., 2011). A recent computational model and the cryo-EM structure of the KCNQ1-KCNE3-calmodulin (CaM) complex clearly showed that KCNE3 interacts with the S1 segment and the pore domain (Kroncke et al., 2016; Sun and MacKinnon, 2020). However, the mechanism by which KCNE3 retains the KCNQ1 VSD at a specific position is still not clearly understood.

In this work, by taking advantage of the cryo-EM structure of the KCNQ1-KCNE3-CaM complex (Sun and MacKinnon, 2020) and by mutating several amino acid residues on either KCNQ1 and KCNE3, we identified a triad interaction (KCNE3 and the S1/S4 segments of KCNQ1) that is required for retaining the VSD in the intermediate/up positions, probably by preventing the S4 segment from going to the down position. Although most of the mutants disrupted the intermediate/up conformation of the VSD, the functional rescue of KCNQ1 F127A-KCNE3 G73 co-expression strongly supports the idea that the specific interaction between KCNQ1 and KCNE3 is required to retain the intermediate/up state. We also found that M238 and V241 residues of the S4 segment, which are involved in the triad interaction between KCNE3 and KCNQ1, might be involved in the VSD modulation by KCNE1. Our findings successfully unify the results of previous mutagenesis and structural studies on KCNE3 and offer fundamental frameworks of KCNE protein modulation via the VSD.

## Results

### KCNE3 residues in the middle of the transmembrane segment responsible for channel modulation.

The recently determined cryo-EM structure of the KCNQ1-KCNE3-CaM complex revealed that KCNE3 interacts with the S1 segment of KCNQ1 in the middle of the transmembrane segment (Sun and MacKinnon, 2020). In the structure, the side chains of F68, V72, and I76 in KCNE3 face F127 and F130 in the S1 segment of KCNQ1 (Figure 1A-C). We previously reported that F127 and F130 are required for KCNE3 to make KCNQ1 a constitutively open channel (Nakajo and Kubo, 2011). Therefore, we hypothesized that the interactions between the S1 segment and KCNE3 might be crucial for stabilizing the open states. To confirm the functional roles of these amino acid residues of KCNE3, we first created alanine-substituted mutants (F68A, V72A, and I76A) and co-expressed them with KCNQ1 WT. We confirmed the introduced mutations (including A69F and G73L appeared in Figure 3) did not impair the membrane localization of KCNE3 by confocal imaging with mEGFP-tagged constructs (Figure supplement 1). KCNE3 WT shifted the conductance-voltage (G-V) relationship of the KCNQ1 channel in the far-negative direction, resulting in making KCNQ1 a constitutively open channel for the physiological membrane potential range. On the other hand, all the mutants failed to shift the G-V curves (Figure 1D, E). Previous electrophysiological studies demonstrated that KCNE3 influences the voltage sensor movement (Barro-Soria et al., 2017, 2015; Nakajo and Kubo, 2007; Rocheleau and Kobertz, 2008). To investigate whether these mutations of KCNE3 affect the voltage sensor movement, we next performed VCF to monitor the S4 segment. The KCNQ1 channel for VCF (KCNQ1 C214A/G219C; this construct hereafter being referred to as "$KCNQ1_{vcf}$ WT") was labeled at the introduced cysteine residue (G219C) by Alexa Fluor 488 maleimide (Osteen et al., 2012, 2010). $KCNQ1_{vcf}$ WT alone showed a fluorescence-voltage (F-V) relationship that was mostly fitted to a single Boltzmann function and overlapped with its G-V curve

(Figure 1F, G-figure supplement 1). In contrast, $KCNQ1_{vcf}$ WT co-expressed with KCNE3 WT showed a split F-V relationship, and fluorescence changes were observed both in the negative and positive voltages (Figure 1F, G-figure supplement 1). Consequently, the F-V curve of $KCNQ1_{vcf}$ WT-KCNE3 WT does not fit to a single Boltzmann function but instead fits to a double Boltzmann function (Figure 1G-figure supplement 1). These results are consistent with the results of previous VCF studies (Taylor et al., 2020). To quantify the modulation of S4 movement by KCNE3, we introduced a parameter ($\Delta F_{-160mV}/\Delta F_{60mV}$) to compare the change of fluorescence intensity ($\Delta F$) from the holding potential (-90 mV) to the most negative voltage (-160 mV; $\Delta F_{-160mV}$) and most positive voltage (60 mV; $\Delta F_{60mV}$) in our experiments (Figure 1H). If $\Delta F_{-160mV}/\Delta F_{60mV}$ is close to 0, it means that the S4 segment moves only by depolarization, suggesting that most of the VSDs are at the down position at -90 mV. In contrast, if $\Delta F_{-160mV}/\Delta F_{60mV}$ is close to 1 (or larger), there is a substantial S4 movement by hyperpolarization, indicating that the S4 segments may sit at the upper (intermediate or up) positions. $\Delta F_{-160mV}/\Delta F_{60mV}$ of $KCNQ1_{vcf}$ WT alone is almost negligible (0.04 ± 0.01, $n$=5), indicating that most of the S4 segments of the channels are at the down position and move to the upper position with depolarization. In contrast, $\Delta F_{-160mV}/\Delta F_{60mV}$ of $KCNQ1_{vcf}$ WT-KCNE3 WT is about 1 (0.94 ± 0.13, $n$=5), meaning that a substantial number of S4 segments are in the intermediate position and move either with depolarization or hyperpolarization. We then assessed $\Delta F_{-160mV}/\Delta F_{60mV}$ of each KCNE3 mutant co-expressed with $KCNQ1_{vcf}$ WT. All of the mutants showed reduced $\Delta F_{-160mV}/\Delta F_{60mV}$ values (F68A, 0.32 ± 0.03, $n$=5; V72A, 0.35 ± 0.05, $n$=5; I76A, 0.32 ± 0.06, $n$=5), suggesting that these mutations impair the interaction between KCNQ1 and KCNE3 and thereby shift the equilibrium of the S4 segment to the down position (Figure 1F-H-figure supplement 1). In addition, we noticed that the F-V curves for the KCNE3 mutants lost the plateau observed in that for $KCNQ1_{vcf}$ WT-KCNE3 WT and were rather fitted to a single Boltzmann function (Figure 1G-figure supplement 1), again implying that the mutations destabilized

the intermediate position. Overall, KCNE3 residues in the middle of the transmembrane segment are important for channel modulation, probably by preventing the S4 segment from going to the down position.

## Functional coupling between KCNQ1 S1 segment and KCNE3

As we mentioned, KCNQ1 F127A and F130A mutants co-expressed with KCNE3 WT failed to shift the G-V curves in the negative direction (Nakajo et al., 2011). Next, we combined the KCNQ1 S1 alanine mutants with the KCNE3 alanine mutants to test if the volumes of these residues are necessary for the functional interaction (Figure 2). For the KCNQ1 F127A mutant, co-expression with KCNE3 F68A or V72A yielded G-V curves similar to that for KCNE3 WT, implying that F127 of the S1 segment and F68/V72 of KCNE3 are functionally coupled. Co-expression of KCNQ1 F127A and KCNE3 I76A, on the other hand, showed an additively-shifted G-V curve, meaning F127A and I76A are not functionally coupled (Figure 2A, B). The KCNQ1 F130A mutant co-expressed with KCNE3 F68A or I76A yielded negatively shifted G-V curves compared to that for KCNE3 WT, suggesting that F130 of the S1 segment and F68/I76 of KCNE3 are functionally coupled, while KCNE3 V72A slightly positively shifted KCNQ1 F130A, indicating a weaker functional coupling between F130 and V72 compared to that between F130 and F68/I76 (Figure 2C, D). We believe that analysis using the double alanine mutants at least partially confirmed the functional coupling between the S1 segment and KCNE3. To further confirm the functional coupling between the S1 segment and KCNE3, we next introduced bulky residues into the transmembrane segment of KCNE3 to disrupt the interaction between the S1 segment and KCNE3. We then examined whether smaller alanine mutations in the S1 segment of KCNQ1 (F127A or F130A) rescued these bulky residue mutations. As guided by the KCNQ1-KCNE3-CaM complex structure (Sun and MacKinnon, 2020) as well as newly generated models of KCNQ1 S1 and KCNE3 mutants

by Phyre2 server (Kelley et al., 2015), we tested the idea with two candidate pairs (KCNQ1 F127-KCNE3 G73 and KCNQ1 F130-KCNE3 A69) (Figure 3A). We introduced the G73L mutation because KCNE1 has a leucine residue at the same position (Figure 1C). KCNE3 G73L showed voltage-dependent gating, meaning that KCNQ1 is no longer constitutively active (Figure 3B, C-figure supplement 2). We next tested the pair of KCNQ1 F127A-KCNE3 G73L. The pair successfully rescued the G-V relationship comparable to that of KCNQ1 WT-KCNE3 WT (Figure 3B, C-figure supplement 2). Furthermore, $\Delta F_{-160mV}/\Delta F_{60mV}$ of $KCNQ1_{vcf}$ F127A-KCNE3 G73L (0.80 ± 0.04, *n*=5) showed significant recovery compared to that of $KCNQ1_{vcf}$ WT-KCNE3 G73L (0.22 ± 0.03, *n*=5) and that of $KCNQ1_{vcf}$ F127A-KCNE3 WT (0.31 ± 0.04, *n*=5), suggesting that KCNE3 G73L can stabilize the S4 segment of KCNQ1 F127A in the intermediate position to some extent (Figure 3D, E-figure supplement 2). In contrast, the pair of KCNQ1 F130A-KCNE3 A69F did not recover the channel modulation by KCNE3 (Figure 3F, G-figure supplement 2), implying that F130 (or A69) may have another crucial role in KCNE3 modulation (discussed later). Overall, the results demonstrate the importance of the interaction between the S1 segment and KCNE3. Appropriate side-chain volumes at the interaction interface are necessary for functional interaction in the KCNE3 modulation.

**KCNE3 and the S1 segment modulate VSD movement via M238 and V241 of the S4 segment.**

As we have seen, the interactions between the S1 segment of KCNQ1 and KCNE3 are required for the channel's constitutive activity (Figures 1-3). However, how these interactions regulate the movement of the S4 segment is still not clear. We again closely looked at the KCNQ1-KCNE3-CaM complex structure and noticed that KCNE3 (F68, V72, and I76) and F130 of the S1 segment face the bottom half of the S4 segment, especially the side chains of M238 and V241 (Figure 4A) (Sun and

MacKinnon, 2020). Therefore, we created alanine-substituted mutants of the S4 segment (M238A and V241A) one at a time and found that both KCNQ1 M238A and V241A co-expressed with KCNE3 WT attenuated the shift of the G-V curves in the negative direction (Figure 4B, C). We next applied VCF to analyze the VSD movement of M238A and V241A. Both M238A and V241A without KCNE3 showed normal F-V curves and almost a 0 value of $\Delta F_{-160mV}/\Delta F_{60mV}$ (Figure 4D, E-figure supplement 3). On the other hand, in the presence of KCNE3, M238A and V241A mutants showed smaller values of $\Delta F_{-160mV}/\Delta F_{60mV}$ (M238A, 0.35 ± 0.08, *n*=5; V241A, 0.50 ± 0.06, *n*=5) compared to that of KCNQ1 WT (Figure 4F), indicating that some of the VSDs were shifted to the down position from the intermediate position at -90 mV. Therefore, we concluded that M238 and V241 are the sites where the binding of KCNE3 is converted to the VSD movement's modulation. This mechanism may be required to prevent the S4 segment from going to the down position by KCNE3.

**M238 and V241 of the S4 segment are also involved in VSD modulation by KCNE1.**

We also co-expressed KCNQ1 M238A and V241A with KCNE1 to investigate whether these S4 mutants influence the VSD modulation by KCNE1 since previous experiments demonstrated that KCNE1 affects S4 movement (Osteen et al., 2012, 2010). In the presence of KCNE1, M238A and V241A mutants showed the typical $I_{Ks}$-like current and positively-shifted G-V curves (Figure 5A, B). We then examined the VSD movements of these mutants with KCNE1. $KCNQ1_{vcf}$ WT co-expressed with KCNE1 WT showed $\Delta F_{-160mV}/\Delta F_{60mV}$ (0.98 ± 0.04, *n*=5) similar to that of $KCNQ1_{vcf}$ WT co-expressed with KCNE3 WT (0.94 ± 0.13, *n*=5), suggesting that many of the S4 segments of the channels are in the intermediate position at -90 mV as in the case of KCNE3 (Figure 5C-E-figure supplement 4). We then assessed $\Delta F_{-160mV}/\Delta F_{60mV}$ of $KCNQ1_{vcf}$ M238A and V241A co-expressed with KCNE1 WT. Strikingly, $KCNQ1_{vcf}$ M238A and V241A co-expressed with KCNE1 WT also

showed reduced values of $\Delta F_{-160mV}/\Delta F_{60mV}$ of about 0.5 (Figure 5C-E-figure supplement 4), suggesting that both M238A and V241A mutations affect the S4 movement modulated by KCNE1. These results indicate that M238 and V241 in the S4 segment are involved in the VSD modulation for both KCNE1 and KCNE3.

## Discussion

In this work, we conducted site-directed mutational analyses using TEVC and VCF, inspired by the recently determined cryo-EM structures of the KCNQ1-KCNE3-CaM complex (Sun and MacKinnon, 2020). Our main finding is triad interaction formed by KCNE3 with the S1 and S4 segments of KCNQ1. The triad is a key component for the channel modulation by KCNE3, which prevents the S4 segment of the VSD from going to the down position at resting membrane potential. Another interesting finding is that M238 and V241 of the S4 segment in the triad may also be involved in the VSD modulation by KCNE1.

Previous studies demonstrated that “the triplet” of amino acid residues in the middle of the transmembrane segment (“FTL” for KCNE1 and “TVG” for KCNE3) is a structural determinant of KCNE modulation properties (Barro-Soria et al., 2017; Melman et al., 2002, 2001). However, why the triplets determine the modulation type is still not well understood. Besides “the triplet,” our current work showed that a broader range of amino acid residues (F68, V72, and I76), which forms three helical turns in total in the middle of the transmembrane segment of KCNE3, were involved in the interactions among KCNE3 and S1 and S4 segments and were required for maintaining the constitutive activity of the KCNQ1-KCNE3 channel (Figure 1). For the KCNQ1 side, we previously demonstrated that two phenylalanine residues, F127 and F130, in the S1 segment are important for the channel modulation by KCNE3, but how these mutations affect the channel modulation has been unknown (Nakajo et al., 2011). The cryo-EM KCNQ1-KCNE3-CaM structure (PDB: 6V00) clearly

shows that F127 and F130 of the S1 segment face KCNE3 (F68, V72, and I76). We therefore hypothesized that the interaction of these amino acid residues is essential for the KCNE3 function. Our electrophysiology and VCF studies confirmed that the interaction of these amino acid residues is required for proper KCNE3 function, which maintains the opening of the KCNQ1 channel.

Although we mainly introduced alanine mutations to assess the amino acid residue's importance for the interactions (Figure 2), the introduction of bulky amino acid residues at A69 or G73 also disrupted the KCNE3 function, suggesting that an appropriate distance between the S1 segment and KCNE3 is required (Figure 3). The rescue of KCNE3 G73L by KCNQ1 F127A also supports that idea (Figure 3B-E). In contrast, the pair of KCNQ1 F130A-KCNE3 A69F failed to recover the KCNE3 modulation (Figure 3F, G). One possibility is that the KCNQ1 F130 plays a central role in the triad. F130 interacts not only with KCNE3 (F68 and V72) but also the S4 segment (M238 and V241) in the cryo-EM structure (Sun and MacKinnon, 2020) (Figure 4A), and loss of the benzyl group at F130 may therefore affect the interaction with the S4 segment. F127, on the other hand, only faces KCNE3 in the structure. Therefore, the role of F127 might be only stabilization of the KCNE3 interaction.

According to the results of a study by Taylor *et al.* (Taylor et al., 2020) and the results of our VCF analysis, the F-V curve derived from $KCNQ1_{vcf}$ WT co-expressed with KCNE3 WT is fitted to a double Boltzmann function (Figure 1G-figure supplement 1). This suggests that the S4 segments stay in the intermediate position at resting membrane potential (Holding potential was -90 mV throughout our study.), allowing the S4 segment to move to either the down or up position by hyperpolarization or depolarization. The intermediate state of the KCNQ1 VSD has recently been determined by solution nuclear magnetic resonance (NMR) (Taylor et al., 2020). The structure is a single VSD without the rest of the channel. It clearly demonstrates that the fourth arginine (R237) on the S4 segment is under the charge transfer center (F167), suggesting this is the intermediate state

(Figure 6B). On the other hand, in the VSD of the cryo-EM structure (Sun and MacKinnon, 2020), R237 is located over F167, and the VSD is likely to be in the up position (Figure 6A). In this study, we utilized the cryo-EM structure to confirm that the interaction of KCNE3 and the S1 segment is necessary for the modulation. Subsequently, we identified M238 and V241 of the S4 segment, again by utilizing the cryo-EM structure. In the intermediate state structure, M238 and V241 are still directed towards F130, although M238 is slightly closer to F130 and V241 is slightly away from F130 (Figure 6B). The intermediate state likely dominates at the holding potential of -90 mV. If that is the case, the locations of M238 and V241 in the intermediate state indicate that they can still play a pivotal role in maintaining the VSD in the intermediate position.

We showed that M238 and V241 of the S4 segment also play a pivotal role in channel modulation by KCNE1 (Figure 5). According to the ionic currents and the G-V curves of M238A and V241A mutants, alanine-substituted mutants of these residues (M238A and V241A) showed more severe effects on the pore gating modulation by KCNE3 than that by KCNE1. However, they showed similar effects on the $\Delta F_{-160mV}/\Delta F_{60mV}$ values (Figure 4D, F, 5C, E), suggesting that the VSDs are no longer stabilized at the intermediate position in both cases. Because KCNE1 specifically suppresses the intermediate-open (IO) state (Hou et al., 2017), the KCNQ1-KCNE1 channel must enter a fully activated open state (AO) to be conductive. Therefore, destabilization of the intermediate state by M238A or V241A may not substantially affect the ionic currents for the KCNQ1-KCNE1 channel. On the other hand, the KCNQ1-KCNE3 channel is conductive at the IO state; therefore, ionic currents appear to be significantly affected by M238A and V241A. Thus, the modulation of VSD movement by KCNE1 and KCNE3 might share a common mechanism of stabilization of the intermediate state through M238 and V241.

One drawback of this kind of mutation study is that the impairment of mutations could occur at different stages, such as expression, binding, or modulation efficacy. We confirmed that the

membrane localization of KCNE3 mutants was not impaired with mEGFP-tagged KCNE3 constructs (Figure supplement 1). Still, it remains unknown which stage is more responsible for the outcome between the binding affinity or the modulation efficacy in each KCNE3 mutant. Some KCNE3 mutants produced different effects on different KCNQ1 mutants; for example, KCNE3 F68A mutant positively shifted the G-V relationship of KCNQ1 F127A and negatively shifted that of KCNQ1 F130A (Figure 2). The rescue experiment in Figure 3 also indicates KCNE3 G73L effectively alters gating behavior. Therefore, we believe most of the KCNE3 mutants in this study affect the modulation, not the binding.

In summary, our results demonstrate that the triad interactions of KCNE3 with the S1 and S4 segments of the KCNQ1 channel (Figure 4A) are required for retaining the VSD in the intermediate position, probably by preventing the S4 segment from going to the down position, thereby keeping the KCNQ1-KCNE3 channels constitutively active.

## Materials and Methods

### Expression in *Xenopus laevis* oocytes

The human KCNQ1 (NCBI Accession Number NP_000209.2; WT and mutants) and mouse KCNE3 (NP_001177798; WT and mutants) and human KCNE1 (HsKCNE1, NP_000210) genes were cloned into the pGEMHE expression vector (Liman et al., 1992). The cRNAs were transcribed using mMESSAGE mMACHINE™ T7 Transcription Kits (Thermo Fisher Scientific, AM1344). Oocytes were surgically removed from female *Xenopus laevis* frogs anesthetized in water containing 0.1% tricaine (Sigma-Aldrich, E10521) for 15-30 min. The oocytes were treated with collagenase (Sigma-Aldrich, C0130) for 6-7 h at room temperature to remove the follicular cell layer. Defolliculated oocytes of similar sizes at stage V or VI were selected, microinjected with 50 nl of cRNA solution (10 ng for KCNQ1, and 1 ng for KCNE3 and KCNE1) using a NANOJECT II (Drummond Scientific Co.), and incubated until use at 18 °C in MBSH buffer (88 mM NaCl, 1 mM KCl, 2.4 mM $NaHCO_3$, 10 mM HEPES, 0.3 mM $Ca(NO_3)_2$, 0.41 mM $CaCl_2$, and 0.82 mM $MgSO_4$, pH 7.6) supplemented with 0.1% penicillin-streptomycin solution (Sigma-Aldrich, P4333). All experiments were approved by the Animal Care Committee of Jichi Medical University (Japan) under the protocol no. 18027-03 and were performed following the institutional guidelines.

### Two-electrode voltage-clamp

cRNA-injected oocytes were incubated for 2-3 days. Ionic currents were recorded with a two-electrode voltage clamp using an OC-725C amplifier (Warner Instruments) at room temperature. The bath chamber was perfused with $Ca^{2+}$-free ND96 solution (96 mM NaCl, 2 mM KCl, 2.8 mM $MgCl_2$, 5 mM HEPES, pH 7.6) supplemented with 100 μM $LaCl_3$ to block endogenous hyperpolarization-activated currents (Osteen et al., 2010). The microelectrodes were drawn from borosilicate glass capillaries (Harvard Apparatus, GC150TF-10) using a P-1000 micropipette puller (Sutter Instrument) to a resistance of 0.2–1.0 MΩ and filled with 3 M KCl. Currents were elicited

from the holding potential of -90 mV to steps ranging from -100 to +60 mV in +20-mV steps each for 2 sec with 5-sec intervals (or 10-sec intervals for KCNQ1-KCNE1 currents). Generation of voltage-clamp protocols and data acquisition were performed using a Digidata 1550 interface (Molecular Devices) controlled by pCLAMP 10.7 software (Molecular Devices). Data were sampled at 10 kHz and filtered at 1 kHz.

### Voltage dependence analysis

G–V relationships were taken from tail current amplitude at -30 mV fitted using pCLAMP 10.7 software (Molecular Devices) to a two-state Boltzmann equation:

$$G = G_{min} + (G_{max} - G_{min}) / (1+e^{-zF(V - V_{1/2}) / RT}),$$

where $G_{max}$ and $G_{min}$ are the maximum and minimum tail current amplitudes, respectively, z is the effective charge, $V_{1/2}$ is the half-activation voltage, T is the temperature in degrees Kelvin, F is Faraday's constant, and R is the Boltzmann constant. $G/G_{max}$, which is the normalized tail current amplitude, was plotted against membrane potential for presentation of the G–V relationships. Gating parameters obtained in this study are listed in Table supplement 1.

### Voltage-clamp fluorometry

Sample preparation, data acquisition, and data analysis were performed similarly as described previously (Nakajo and Kubo, 2014). cRNA-injected oocytes were incubated for 4-5 days, labeled for 30 min with 5 μM Alexa Fluor™ 488 $C_5$ maleimide (Thermo Fisher Scientific, A10254) in high potassium KD98 solution (98 mM KCl, 1.8 mM $CaCl_2$, 1 mM $MgCl_2$, 5 mM HEPES, pH 7.6) (Nakajo and Kubo, 2014; Osteen et al., 2010), and washed with $Ca^{2+}$-free ND96 solution to remove unreacted Alexa probes. The bath chamber was filled with $Ca^{2+}$-free ND96 solution supplemented with 100 μM $LaCl_3$. The microelectrodes were drawn from borosilicate glass capillaries (Harvard Apparatus, GC150TF-15). Currents were elicited from the holding potential of -90 mV to steps ranging from +60 to -160 mV in -20-mV steps each for 2 sec with 20-sec intervals. Generation of

voltage-clamp protocols and data acquisition were performed using a Digidata 1440A interface (Molecular Devices) controlled by pCLAMP 10.7 software (Molecular Devices). Data were sampled at 10 kHz and filtered at 1 kHz. Fluorescence recordings were performed with a macro zoom microscope MVX10 (Olympus) equipped with a 2x objective lens (MVPLAPO 2XC, NA = 0.5, Olympus), 2x magnification changer (MVX-CA2X, Olympus), GFP filter cube (U-MGFPHQ/XL, Olympus), and an XLED1 LED light source with a BDX (450-495 nm) LED module (Excelitas Technologies). Fluorescence signals were obtained by using a photomultiplier (H10722-110; Hamamatsu Photonics) and digitized at 1 kHz through Digidata1440, filtered at 50 Hz, and recorded using pClamp10 simultaneously with ionic currents. The shutter for the excitation was open during the recording, which induced a continuous decrease of fluorescence due to photobleaching. Therefore, we calculated the bleaching rate for each experiment using the baseline levels of the initial 1100 ms before test pulses of each trace and compensated the fluorescence traces by subtracting the bleached component calculated from each trace's bleaching rate (R), assuming that the fluorescence was linearly decreased. Arithmetic operations were performed with Clampfit software from pClamp10.

[Compensated trace] = [recorded trace] x (1 – (R x [time]) (Nakajo and Kubo, 2014),

where [time] is the time value of the point given by Clampfit. We then normalized the fluorescence traces by setting each baseline level to 1.

**VCF analysis**

F–V relationships were taken from the fluorescence change from the baseline (ΔF) plotted against membrane potential. ΔF values were then normalized by $\Delta F_{60mV}$ for the normalized F-V relationships shown in Figures 1G, 4E and 5D. F–V relationships were fitted using Igor Pro software (WaveMatrices Co.) to a double Boltzmann equation:

$$F = F_{min} + (F_1 - F_{min}) / (1+e^{-z_1F(V - V_{1/2(F1)}) / RT}) + (F_2 - F_1) / (1+e^{-z_2F(V - V_{1/2(F2)}) / RT}),$$

where $F_1$, $F_2$ and $F_{min}$ are the first, second, and baseline fluorescence components, z1 and z2 are the effective charges for each fluorescence component, $V_{1/2(F1)}$ and $V_{1/2(F2)}$ are the half-activation voltage for each fluorescence component, T is the temperature in degrees Kelvin, F is Faraday's constant, and R is the Boltzmann constant.

### Conforcal Microscopy

The C-terminally mEGFP-tagged mouse KCNE3 WT and mutants (or mEGFP alone) were co-injected with the human KCNQ1 WT in oocytes (10 ng for KCNQ1, and 1 ng for KCNE3-mEGFP or mEGFP). mEGFP was fused to KCNE3 with a flexible GSS linker (Nakajo et al., 2010). The oocytes were imaged using an FV1000 confocal laser scanning microscope (Olympus) with 10x objective lens.

### Statistical analysis

The data were expressed as mean±s.e.m. Differences between WT and mutants were evaluated by Dunnett's test with EZR software (Kanda, 2013).

## Acknowledgments

We thank Dr. Yuichiro Fujiwara (Kagawa University) and the Nakajo laboratory members for their valuable discussions, Dr. Tom Kouki (Jichi Medical University) for technical support on confocal microscopy. This work was supported by the Japan Society for the Promotion of Science (JSPS) KAKENHI (Grant Nos. 19K23833 and 20H03200 to G.K. and 17K08552 to K.N.) and by JICHI MEDICAL UNIVERSITY YOUNG INVESTIGATOR AWARD to G.K.

## References

Abbott GW. 2016. KCNE1 and KCNE3: the yin and yang of voltage-gated K+ channel regulation. *Gene* **576**:1–13. doi:10.1016/j.gene.2015.09.059.

Aggarwal SK, MacKinnon R. 1996. Contribution of the S4 segment to gating charge in the Shaker K+ channel. *Neuron* **16**:1169–1177. doi:10.1016/S0896-6273(00)80143-9

Barhanin J, Lesage F, Guillemare E, Fink M, Lazdunski M, Romey G. 1996. KvLQT1 and lsK (minK) proteins associate to form the IKs cardiac potassium current. *Nature* **384**:78–80.

Barro-Soria R, Perez ME, Larsson HP. 2015. KCNE3 acts by promoting voltage sensor activation in KCNQ1. *Proc Natl Acad Sci U S A* **112**:E7286–E7292. doi:10.1073/pnas.1516238112

Barro-Soria R, Ramentol R, Liin SI, Perez ME, Kass RS, Larsson HP. 2017. KCNE1 and KCNE3 modulate KCNQ1 channels by affecting different gating transitions. *Proc Natl Acad Sci U S A* **114**:E7367–E7376. doi:10.1073/pnas.1710335114

Barro-Soria R, Rebolledo S, Liin SI, Perez ME, Sampson KJ, Kass RS, Larsson HP. 2014. KCNE1 divides the voltage sensor movement in KCNQ1/KCNE1 channels into two steps. *Nat Commun* **5**. doi:10.1038/ncomms4750

Bendahhou S, Marionneau C, Haurogne K, Larroque MM, Derand R, Szuts V, Escande D, Demolombe S, Barhanin J. 2005. In vitro molecular interactions and distribution of KCNE family with KCNQ1 in the human heart. *Cardiovasc Res* **67**:529–538. doi:10.1016/j.cardiores.2005.02.014

Catterall WA. 1988. Structure and Function of Voltage-Sensitive Ion Channels. *Science* **242**:50–61. doi:10.1126/science.2459775.

Chung DY, Chan PJ, Bankston JR, Yang L, Liu G, Marx SO, Karlin A, Kass RS. 2009. Location of KCNE1 relative to KCNQ1 in the IKS potassium channel by disulfide cross-linking of substituted cysteines. *Proc Natl Acad Sci U S A* **106**:743–748. doi:10.1073/pnas.0811897106

Fedida D, Hesketh JC. 2001. Gating of voltage-dependent potassium channels. *Prog Biophys Mol Biol*

**75**:165–199. doi:10.1016/S0079-6107(01)00006-2

Grahammer F, Herling AW, Lang HJ, Schmitt-Gräff A, Wittekindt OH, Nitschke R, Bleich M, Barhanin J, Warth R. 2001. The cardiac K+ channel KCNQ1 is essential for gastric acid secretion. *Gastroenterology* **120**:1363–1371. doi:10.1053/gast.2001.24053

Hou P, Eldstrom J, Shi J, Zhong L, McFarland K, Gao Y, Fedida D, Cui J. 2017. Inactivation of KCNQ1 potassium channels reveals dynamic coupling between voltage sensing and pore opening. *Nat Commun* **8**:1–11. doi:10.1038/s41467-017-01911-8

Jensen MØ, Jogini V, Borhani DW, Leffler AE, Dror RO, Shaw DE. 2012. Mechanism of voltage gating in potassium channels. *Science (80- )* **336**:229–233. doi:10.1126/science.1216533

Kanda Y. 2013. Investigation of the freely available easy-to-use software "EZR" for medical statistics. *Bone Marrow Transplant* **48**:452–458. doi:10.1038/bmt.2012.244

Kang C, Tian C, Sönnichsen FD, Smith JA, Meiler J, George AL, Vanoye CG, Hak JK, Sanders CR. 2008. Structure of KCNE1 and implications for how it modulates the KCNQ1 potassium channel. *Biochemistry* **47**:7999–8006. doi:10.1021/bi800875q

Kelley LA, Mezulis S, Yates CM, Wass MN, Sternberg MJE. 2015. The Phyre2 web portal for protein modeling, prediction and analysis. *Nat Protoc* **10**:845–858. doi:10.1038/nprot.2015.053

Kroncke BM, Van Horn WD, Smith J, Kang C, Welch RC, Song Y, Nannemann DP, Taylor KC, Sisco NJ, George AL, Meiler J, Vanoye CG, Sanders CR. 2016. Structural basis for KCNE3 modulation of potassium recycling in epithelia. *Sci Adv* **2**. doi:10.1126/sciadv.1501228

Larsson HP, Baker OS, Dhillon DS, Isacoff EY. 1996. Transmembrane movement of the Shaker K+ channel S4. *Neuron* **16**:387–397. doi:10.1016/S0896-6273(00)80056-2

Liman E, Tytgat J, Hess P. 1992. Subunit stoichiometry of a mammalian K+ channel determined by construction of multimeric cDNAs. *Neuron* **9**:861–871.

Liman ER, Hess P. 1991. Voltage-sensing residues in the S4 region of a mammalian K+ channel. *Nature*

**353**:752–756. doi:10.1038/353752a0

Logothetis DE, Movahedi S, Satler C, Lindpaintner K, Nadal-Ginard B. 1992. Incremental reductions of positive charge within the S4 region of a voltage-gated K+ channel result in corresponding decreases in gating charge. *Neuron* **8**:531–540. doi:10.1016/0896-6273(92)90281-H

Long SB, Campbell EB, MacKinnon R. 2005. Crystal structure of a mammalian voltage-dependent Shaker family K + channel. *Science* **309**:897–903. doi:10.1126/science.1116269

Mannuzzu LM, Moronne MM, Isacoff EY. 1996. Direct physical measure of conformational rearrangement underlying potassium channel gating. *Science* **271**:213–216. doi:10.1126/science.271.5246.213

Melman YF, Domènech A, De la Luna S, McDonald T V. 2001. Structural Determinants of KvLQT1 Control by the KCNE Family of Proteins. *J Biol Chem* **276**:6439–6444. doi:10.1074/jbc.M010713200

Melman YF, Krumerman A, McDonald T V. 2002. A single transmembrane site in the KCNE-encoded proteins controls the specificity of KvLQT1 channel gating. *J Biol Chem* **277**:25187–25194. doi:10.1074/jbc.M200564200

Nakajo K. 2019. Gating modulation of the KCNQ1 channel by KCNE proteins studied by voltage-clamp fluorometry **16**:121–126. doi:10.2142/biophysico.16.0_121

Nakajo K, Kubo Y. 2014. Steric hindrance between S4 and S5 of the KCNQ1/KCNE1 channel hampers pore opening. *Nat Commun* **5**. doi:10.1038/ncomms5100

Nakajo K, Kubo Y. 2007. KCNE1 and KCNE3 Stabilize and/or Slow Voltage Sensing S4 Segment of KCNQ1 Channel. *J Gen Physiol* **130**:269–281. doi:10.1085/jgp.200709805

Nakajo K, Nishino A, Okamura Y, Kubo Y. 2011. KCNQ1 subdomains involved in KCNE modulation revealed by an invertebrate KCNQ1 orthologue. *J Gen Physiol* **138**:521–535. doi:10.1085/jgp.201110677

Nakajo K, Ulbrich MH, Kubo Y, Isacoff EY. 2010. Stoichiometry of the KCNQ1 - KCNE1 ion channel complex. *Proc Natl Acad Sci* **107**:18862–18867. doi:10.1073/pnas.1010354107

Noda M, Shimizu S, Tanabe T, Takai T, Kayano T, Ikeda T, Takahashi H, Nakayama H, Kanaoka Y, Minamino N, Kangawa K, Matsuo H, Raftery MA, Hirose T, Inayama S, Hayashida H, Miyata T, Numa S. 1984. Primary structure of Electrophorus electricus sodium channel deduced from cDNA sequence. *Nature* **312**:121–127. doi:10.1038/312121a0

Osteen JD, Barro-Soria R, Robey S, Sampson KJ, Kass RS, Larsson HP. 2012. Allosteric gating mechanism underlies the flexible gating of KCNQ1 potassium channels. *Proc Natl Acad Sci U S A* **109**:7103–7108. doi:10.1073/pnas.1201582109

Osteen JD, Gonzalez C, Sampson KJ, Iyer V, Rebolledo S, Larsson HP, Kass RS. 2010. KCNE1 alters the voltage sensor movements necessary to open the KCNQ1 channel gate. *Proc Natl Acad Sci U S A* **107**:22710–22715. doi:10.1073/pnas.1016300108

Papazian DM, Timpe LC, Jan YN, Jan LY. 1991. Alteration of voltage-dependence of Shaker potassium channel by mutations in the S4 sequence. *Nature* **349**:305–310. doi:10.1038/349305a0

Preston P, Wartosch L, Günzel D, Fromm M, Kongsuphol P, Ousingsawat J, Kunzelmann K, Barhanin J, Warth R, Jentsch TJ. 2010. Disruption of the K+ channel β-subunit KCNE3 reveals an important role in intestinal and tracheal Cl- transport. *J Biol Chem* **285**:7165–7175. doi:10.1074/jbc.M109.047829

Rocheleau JM, Kobertz WR. 2008. KCNE peptides differently affect voltage sensor equilibrium and equilibration rates in KCNQ1 K+ channels. *J Gen Physiol* **131**:59–68. doi:10.1085/jgp.200709816

Sanguinetti MC, Curran ME, Zou A, Shen J, Spector PS, Atkinson DL, Keating MT. 1996. Coassembly of K(V)LQT1 and minK (IsK) proteins to form cardiac I(Ks) potassium channel. *Nature* **384**:80–83. doi:10.1038/384080a0

Schroeder BC, Waldegger S, Fehr S, Bleich M, Warth R, Greger R, Jentsch TJ. 2000. A constitutively open potassium channel formed by KCNQ1 and KCNE3. *Nature* **403**:196–199. doi:10.1038/35003200

Sun J, MacKinnon R. 2020. Structural Basis of Human KCNQ1 Modulation and Gating. *Cell* **180**:340–347. doi:10.1016/j.cell.2019.12.003

Takumi T, Ohkubo H, Nakanishi S. 1988. Cloning of a membrane protein that induces a slow voltage-gated potassium current. *Science* **242**:1042–1045. doi:10.1126/science.3194754

Taylor KC, Kang PW, Hou P, Yang N Du, Kuenze G, Smith JA, Shi J, Huang H, White KM, Peng D, George AL, Meiler J, McFeeters RL, Cui J, Sanders CR. 2020. Structure and physiological function of the human KCNQ1 channel voltage sensor intermediate state. *Elife* **9**:1–31. doi:10.7554/eLife.53901

Van Horn WD, Vanoye CG, Sanders CR. 2011. Working model for the structural basis for KCNE1 modulation of the KCNQ1 potassium channel. *Curr Opin Struct Biol* **21**:283–291. doi:10.1016/j.sbi.2011.01.001

Wang Y, Eldstrom J, Fedida D. 2020. Gating and Regulation of KCNQ1 and KCNQ1 + KCNE1 Channel Complexes. *Front Physiol* **11**:1–21. doi:10.3389/fphys.2020.00504

Xu L, Jiang M, Hsu KL, Zhang M, Tseng GN. 2008. KCNQ1 and KCNE1 in the IKs channel complex make state-dependent contacts in their extracellular domains. *J Gen Physiol* **131**:589–603. doi:10.1085/jgp.200809976

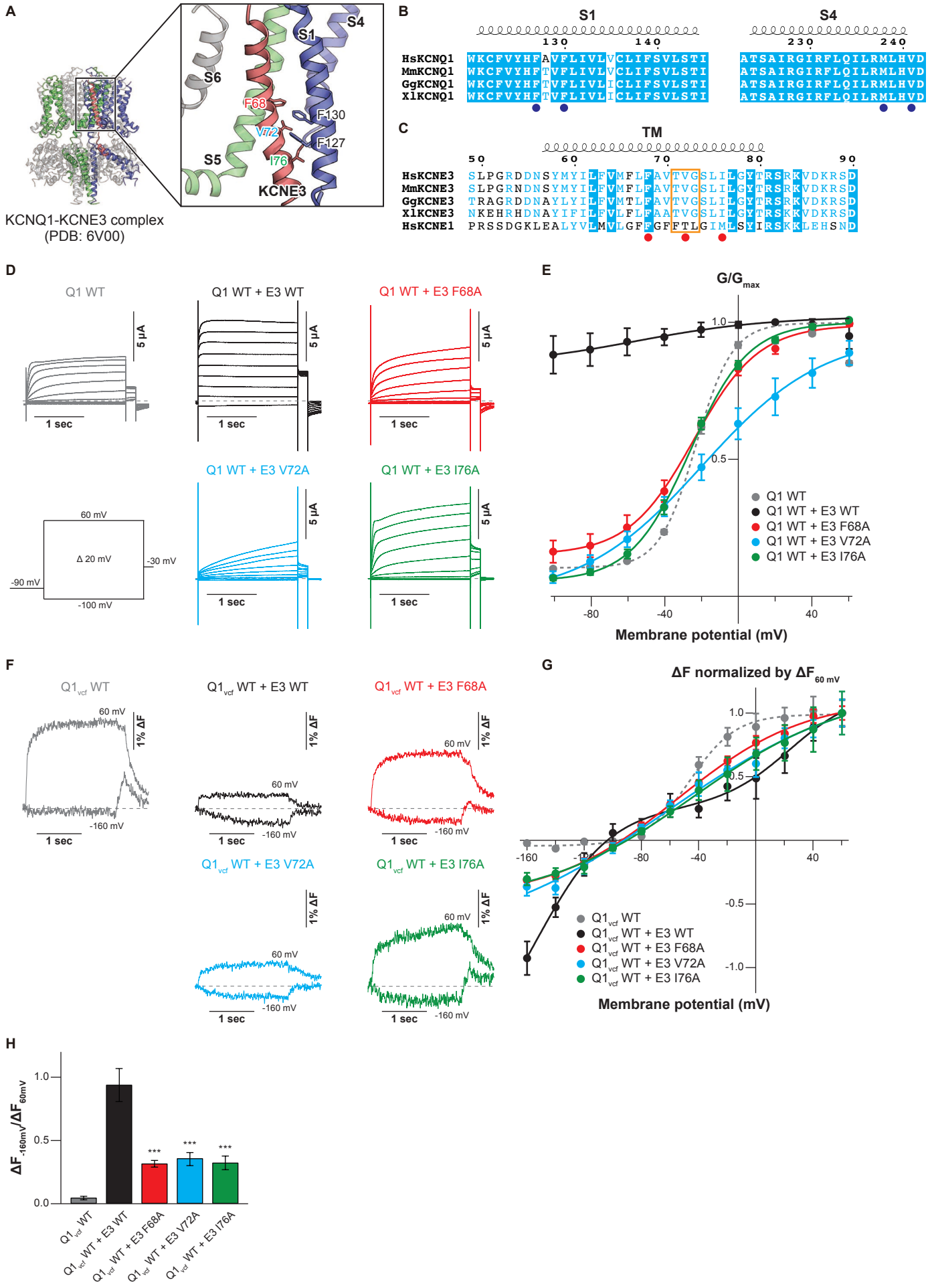
A
S1
S4
S6
F68
F130
V72
F127
S5
I76
KCNE3
KCNQ1-KCNE3 complex
(PDB: 6V00)
B
S1
S4
HsKCNQ1
MmKCNQ1
GgKCNQ1
XlKCNQ1
C
TM
HsKCNE3
MmKCNE3
GgKCNE3
XlKCNE3
HsKCNE1
D
Q1 WT
Q1 WT + E3 WT
Q1 WT + E3 F68A
Q1 WT + E3 V72A
Q1 WT + E3 I76A
5 µA
1 sec
60 mV
Δ 20 mV
-30 mV
-90 mV
-100 mV
E
G/G max
1.0
0.5
-80
-40
40
Membrane potential (mV)
Q1 WT
Q1 WT + E3 WT
Q1 WT + E3 F68A
Q1 WT + E3 V72A
Q1 WT + E3 I76A
F
Q1vcf WT
Q1vcf WT + E3 WT
Q1vcf WT + E3 F68A
Q1vcf WT + E3 V72A
Q1vcf WT + E3 I76A
60 mV
-160 mV
1% ΔF
1 sec
G
ΔF normalized by ΔF 60 mV
1.0
0.5
-0.5
-1.0
-160
-80
-40
40
Membrane potential (mV)
Q1vcf WT
Q1vcf WT + E3 WT
Q1vcf WT + E3 F68A
Q1vcf WT + E3 V72A
Q1vcf WT + E3 I76A
H
ΔF-160mV/ΔF60mV
1.0
0.5
0.0
***
Q1vcf WT
Q1vcf WT + E3 WT
Q1vcf WT + E3 F68A
Q1vcf WT + E3 V72A
Q1vcf WT + E3 I76A

**Figure 1. Functional effects of KCNE3 TM mutants on KCNQ1 modulation.**

(**A**) Close-up view of the interface between KCNQ1 and KCNE3 in the KCNQ1-KCNE3-CaM complex structure (PDB: 6V00). Three KCNQ1 subunits are colored in blue, green, and gray. A KCNE3 subunit is colored in red. The residues involved in the KCNQ1-KCNE3 interaction are depicted by stick models. The molecular graphics were illustrated with CueMol (http://www.cuemol.org/). (**B, C**) Sequence alignment around the S1 and S4 segments of KCNQ1 (B) and the TM segments of KCNE3 and KCNE1 (C). Amino acid sequences were aligned using Clustal Omega (Madeira et al., 2019) and are shown using ESPript3 (Robert and Gouet, 2014). KCNQ1 residues focused on in this work are highlighted with blue dots. KCNE3 residues focused on in this work and "the triplet" (Melman et al., 2002, 2001) are highlighted with red dots and an orange square, respectively. For sequence alignment, human KCNQ1 (HsKCNQ1, NCBI Accession Number: NP_000209), mouse KCNQ1 (MmKCNQ1, NP_032460), chicken KCNQ1 (GgKCNQ1, XP_421022), *Xenopus* KCNQ1 (XlKCNQ1, XP_018111887), human KCNE3 (HsKCNE3, NP_005463), mouse KCNE3 (MmKCNE3, NP_001177798), chicken KCNE3 (GgKCNE3, XP_003640673), *Xenopus* KCNE3 (XlKCNE3 NP_001082346), and human KCNE1 (HsKCNE1, NP_000210) were used. (**D, E**) Representative current traces (D) and G-V relationships (E) of KCNQ1 WT alone as well as KCNQ1 WT in the presence of KCNE3 WT or one of the mutants. Error bars indicate ±s.e.m. for $n$ = 9-10 in (E). (**F**) Representative fluorescence traces of $KCNQ1_{vcf}$ WT alone as well as $KCNQ1_{vcf}$ WT in the presence of KCNE3 WT or one of the mutants. (**G**) F-V relationships of $KCNQ1_{vcf}$ WT alone as well as $KCNQ1_{vcf}$ WT in the presence of KCNE3 WT or one of the mutants normalized by the change of fluorescence intensity at 60 mV ($\Delta F_{60mV}$). Error bars indicate ±s.e.m. for $n$ = 5. (**H**) Ratios of fluorescence change at -160 mV and 60 mV ($\Delta F_{-160mV}/\Delta F_{60mV}$) of $KCNQ1_{vcf}$ WT alone as well as $KCNQ1_{vcf}$ WT in the presence of KCNE3 WT or one of the mutants. Error bars indicate ±s.e.m. for $n$ = 5, and statistical significance was determined by Dunnett's test. *** denotes $P < 0.001$ for $\Delta F_{-160mV}/\Delta F_{60mV}$ compared to $KCNQ1_{vcf}$ WT-KCNE3 WT.

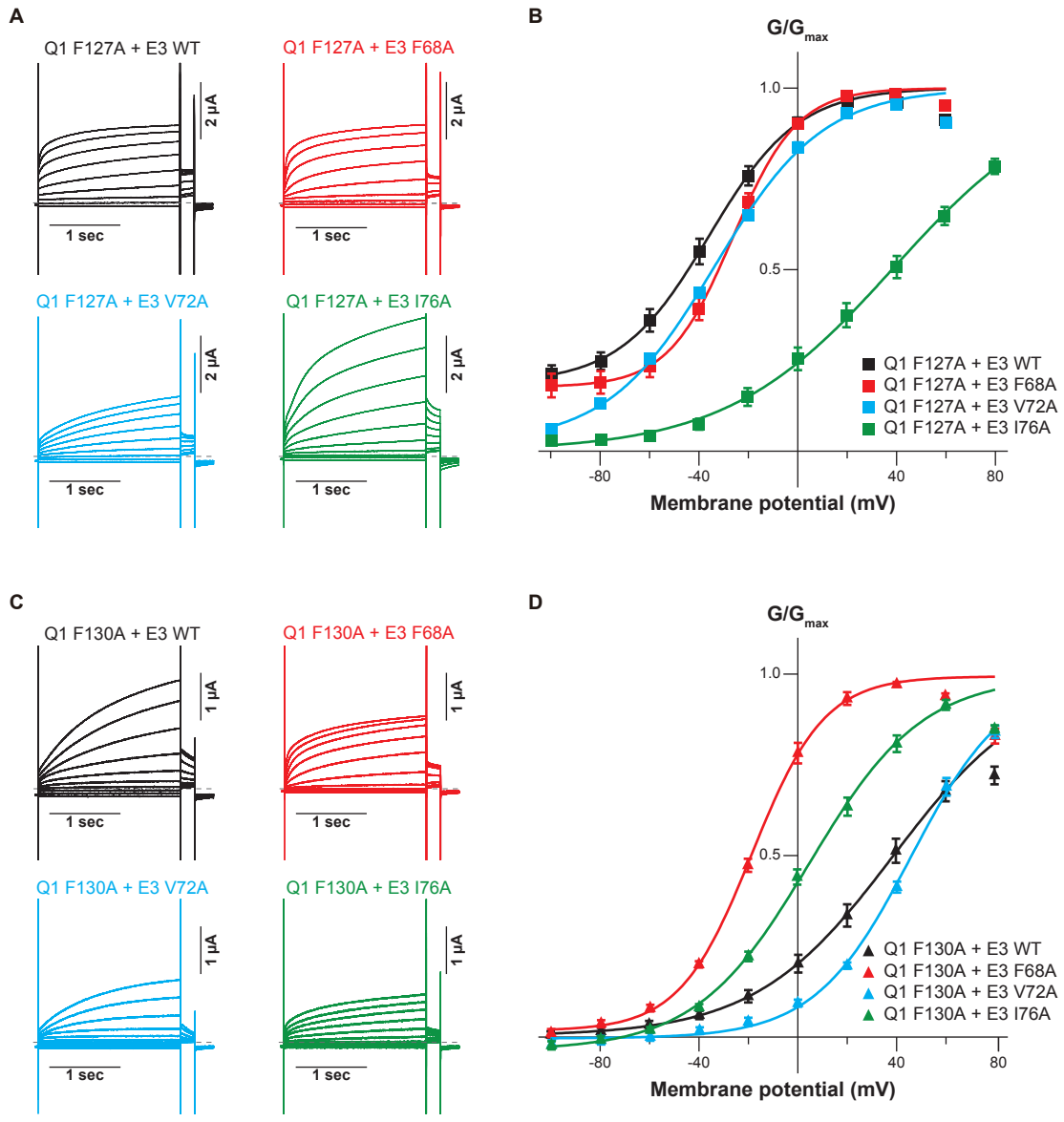


**Figure 2. Effects of the combination of KCNQ1 S1 mutants and KCNE3 TM mutants.**

(**A, B**) Representative current traces (A) and G-V relationships (B) of KCNQ1 F127A-KCNE3 WT, KCNQ1 F127A-KCNE3 F68A, KCNQ1 F127A-KCNE3 V72A, and KCNQ1 F127A-KCNE3 I76A. (**C, D**) Representative current traces (C) and G-V relationships (D) of KCNQ1 F130A-KCNE3 WT, KCNQ1 F130A-KCNE3 F68A, KCNQ1 F130A-KCNE3 V72A, and KCNQ1 F130A-KCNE3 I76A. Error bars indicate ±s.e.m. for $n = 5$ in (B, D).

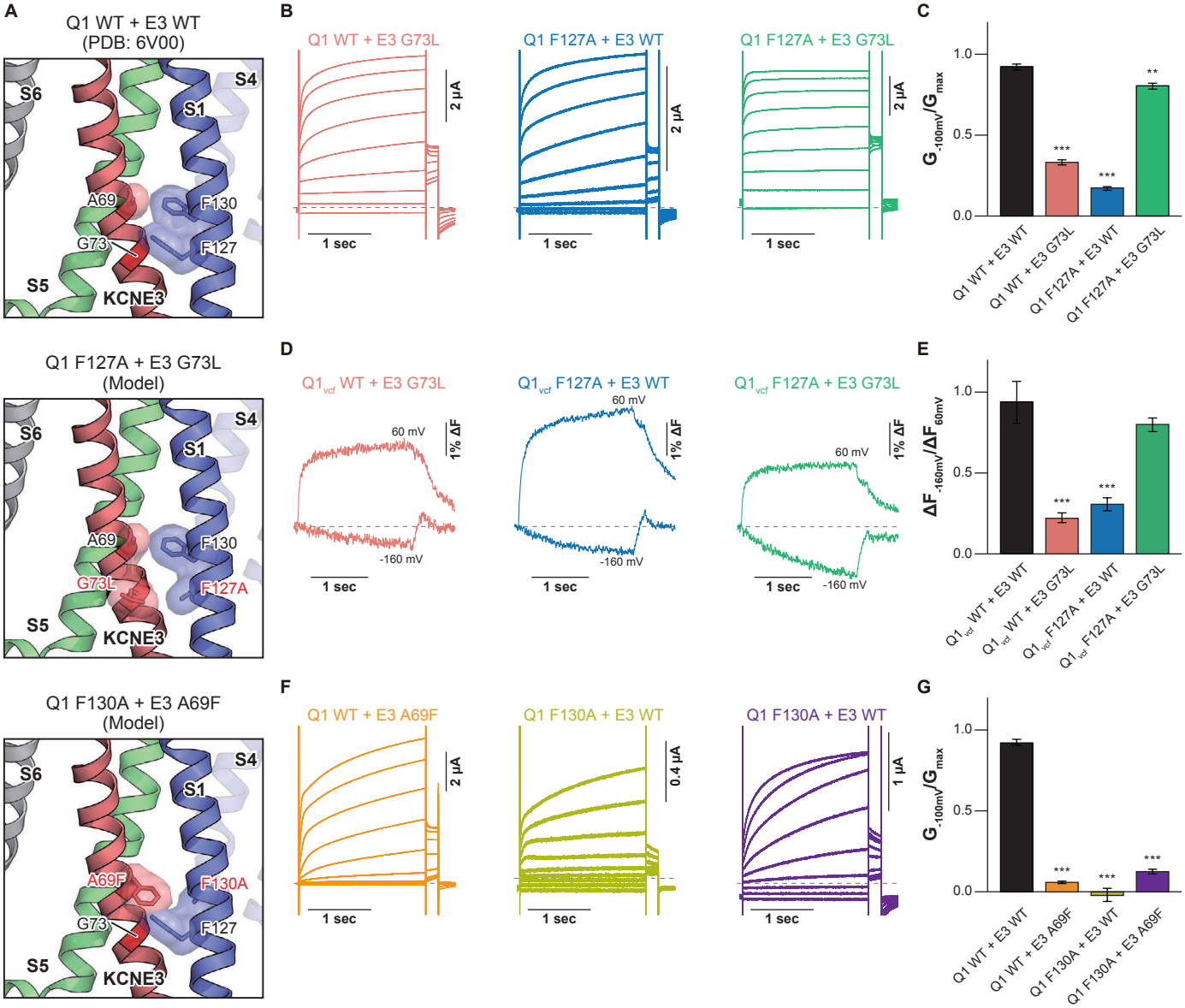


**Figure 3. Appropriate side chain volumes are required for functional interaction between KCNQ1 S1 and KCNE3.**

(**A**) Close-up views of the interface between KCNQ1 S1 and KCNE3 TM in the KCNQ1 WT-KCNE3 WT structure (PDB: 6V00) (up), KCNQ1 F127A-KCNE3 G73L model (middle), and KCNQ1 F130A- KCNE3 A69F model (bottom). KCNQ1 and KCNE3 subunits are colored and depicted according to Figure 1A. Amino acid residues involved in the interaction between KCNE3 and the S1 segment are depicted by the surface models with stick representations. KCNQ1 F127A-KCNE3 G73L and KCNQ1 F130A-KCNE3 A69F models were generated using Phyre2 server (Kelley et al., 2015). (**B, C**) Representative current traces (B) and ratios of conductance at -100 mV and maximum conductance ($G_{-100mV}/G_{max}$) (C) of KCNQ1 WT-KCNE3 G73L, KCNQ1 F127A-KCNE3 WT, and KCNQ1 F127A-KCNE3 G73L. Error bars indicate ±s.e.m. for $n$ = 9-10, and statistical significance was determined by Dunnett's test. ** and *** denote $P < 0.01$ and $P < 0.001$ for $G_{-100mV}/G_{max}$ compared to KCNQ1 WT-KCNE3 WT in (C). (**D, E**) Representative fluorescence traces (D) and ratios of fluorescence changes at -160 mV and at 60 mV ($\Delta F_{-160mV}/\Delta F_{60mV}$) (E) of $KCNQ1_{vcf}$ WT-KCNE3 G73L, $KCNQ1_{vcf}$ F127A-KCNE3 WT, and $KCNQ1_{vcf}$ F127A-KCNE3 G73L. Error bars indicate ±s.e.m. for $n$ = 5, and statistical significance was determined by Dunnett's test. *** denotes $P < 0.001$ for $\Delta F_{-160mV}/\Delta F_{60mV}$ compared to $KCNQ1_{vcf}$ WT-KCNE3 WT in (E). (**F, G**) Representative current traces (F) and ratios of conductance at -100 mV ($G_{-100mV}$) and maximum conductance ($G_{max}$) (G) of KCNQ1 WT-KCNE3 A69F, KCNQ1 F130A-KCNE3 WT, and KCNQ1 F130A-KCNE3 A69F. Error bars indicate ±s.e.m. for $n$ = 9-10, and statistical significance was determined by Dunnett's test. *** denotes $P < 0.001$ for $G_{-100mV}/G_{max}$ compared to KCNQ1 WT-KCNE3 WT in (G).

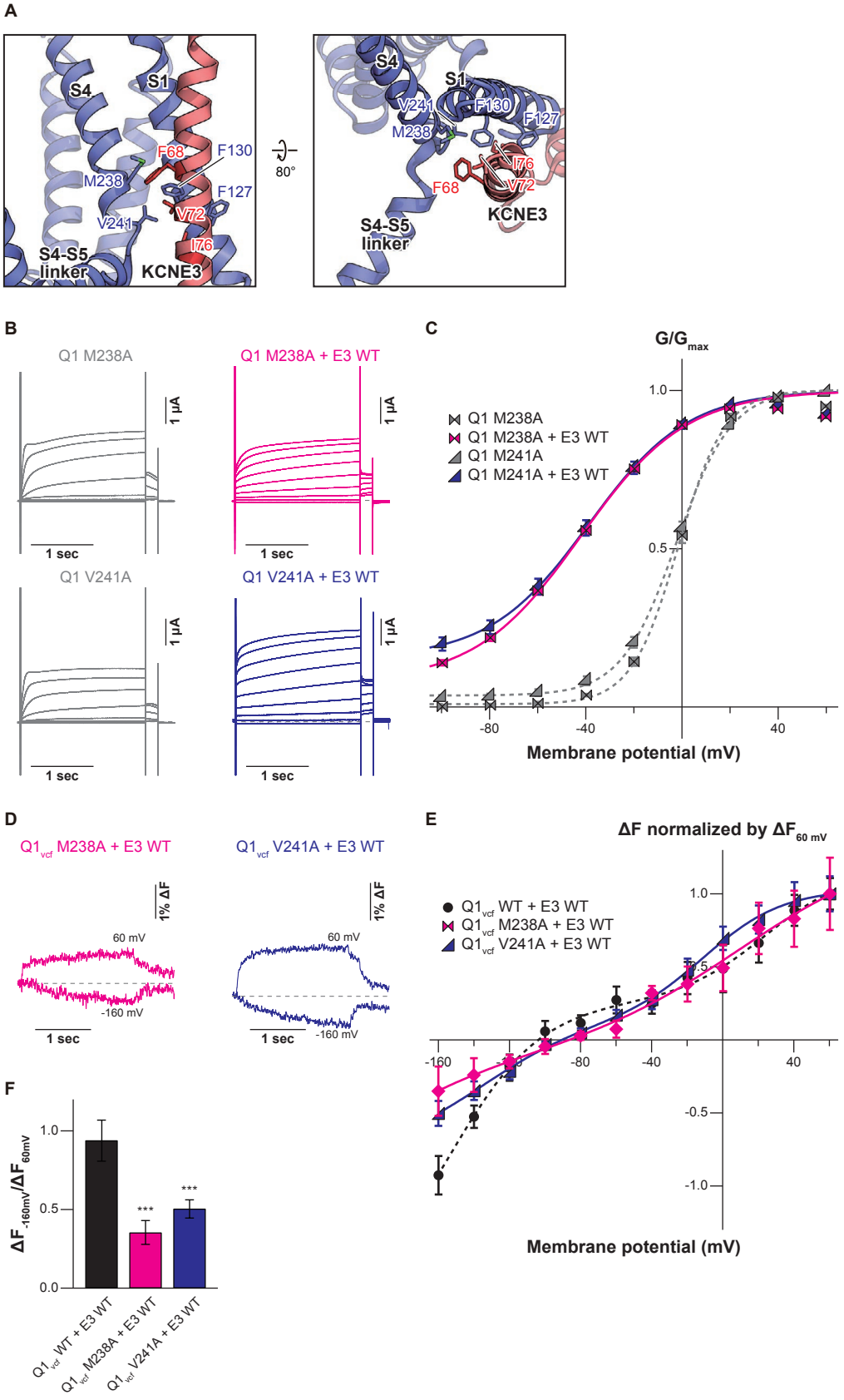
A
S4
S1
F68
F130
M238
F127
V241
V72
I76
S4-S5 linker
KCNE3
80°
B
Q1 M238A
Q1 M238A + E3 WT
Q1 V241A
Q1 V241A + E3 WT
1 μA
1 sec
C
G/Gmax
Q1 M238A
Q1 M238A + E3 WT
Q1 M241A
Q1 M241A + E3 WT
Membrane potential (mV)
D
Q1vcf M238A + E3 WT
Q1vcf V241A + E3 WT
1% ΔF
60 mV
-160 mV
E
ΔF normalized by ΔF60 mV
Q1vcf WT + E3 WT
Q1vcf M238A + E3 WT
Q1vcf V241A + E3 WT
Membrane potential (mV)
F
ΔF-160mV/ΔF60mV
***

**Figure 4. Functional effects of KCNQ1 S4 mutants on KCNQ1 modulation by KCNE3.**

(**A**) Close-up views of the interface between KCNQ1 S4 and KCNE3 TM in the KCNQ1-KCNE3-CaM structure (PDB: 6V00). KCNQ1 and KCNE3 subunits are colored and depicted according to Figure 1A. KCNQ1 and KCNE3 residues are colored blue and red. (**B, C**) Representative current traces (B) and G-V relationships (C) of KCNQ1 M238A, KCNQ1 M238A-KCNE3 WT, KCNQ1 V241A, and KCNQ1 V241A-KCNE3 WT. Error bars indicate ±s.e.m. for $n$ = 9-10 in (C). (**D-F**) Representative fluorescence traces (D), F-V relationships normalized by the change of fluorescence intensity at 60 mV ($\Delta F_{60mV}$) (E), and ratios of fluorescence changes at -160 mV and at 60 mV ($\Delta F_{-160mV}/\Delta F_{60mV}$) (F) of $KCNQ1_{vcf}$ M238A-KCNE3 WT, and $KCNQ1_{vcf}$ V241A-KCNE3 WT. Error bars indicate ±s.e.m. for $n$ = 5 in (E, F). Statistical significance was determined by Dunnett's test. *** denotes $P < 0.001$ for $\Delta F_{-160mV}/\Delta F_{60mV}$ compared to $KCNQ1_{vcf}$ WT-KCNE3 WT using in (F).

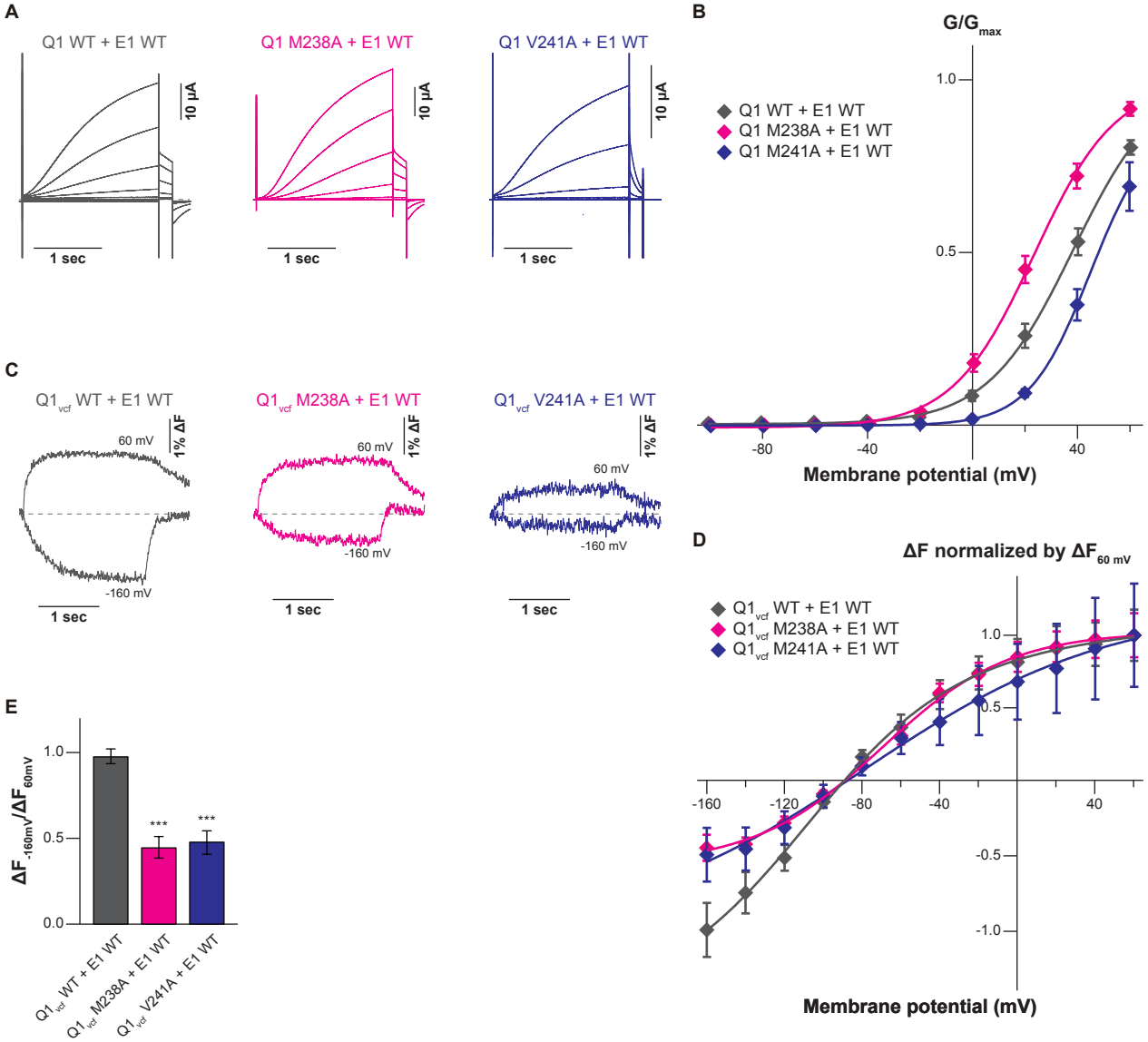


**Figure 5. Functional effects of KCNQ1 S4 mutants on KCNQ1 modulation by KCNE1.**

(**A, B**) Representative current traces (A) and G-V relationships (B) of KCNQ1 WT-KCNE1 WT, KCNQ1 M238A-KCNE1 WT, and KCNQ1 V241A-KCNE1 WT. Error bars indicate ±s.e.m. for $n$ = 9-10 in (D, E). (**C-E**) Representative fluorescence traces (C), F-V relationships normalized by the change of fluorescence intensity at 60 mV ($\Delta F_{60mV}$) (D), and ratios of fluorescence changes at -160 mV and at 60 mV ($\Delta F_{-160mV}/\Delta F_{60mV}$) (E) of $KCNQ1_{vcf}$ WT-KCNE1 WT, $KCNQ1_{vcf}$ M238A-KCNE1 WT, and $KCNQ1_{vcf}$ V241A-KCNE1 WT. Error bars indicate ±s.e.m. for $n$ = 5 in (D, E). Statistical significance was determined by Dunnett's test. *** denotes $P < 0.001$ for $\Delta F_{-160mV}/\Delta F_{60mV}$ compared to $KCNQ1_{vcf}$ WT-KCNE1 WT in (E).

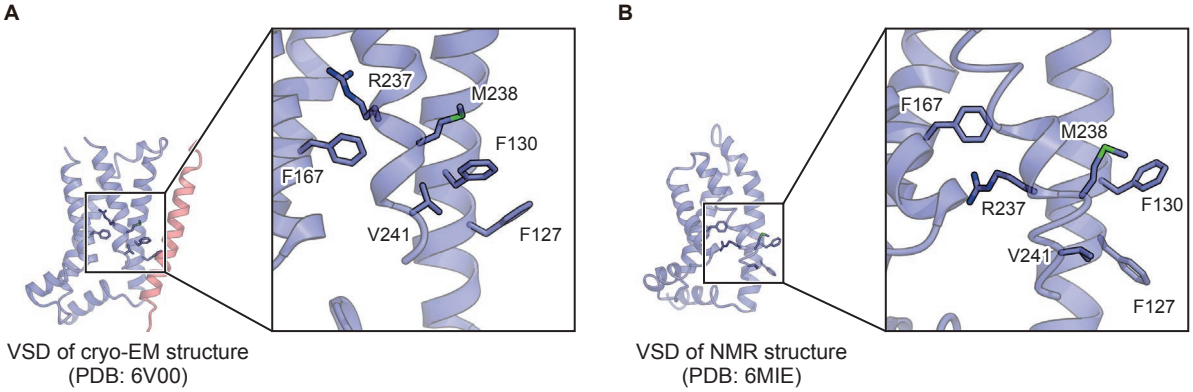


**Figure 6. Structural comparisons of VSDs.**

(**A, B**) VSDs of cryo-EM KCNQ1-KCNE3-CaM (PDB: 6V00) (A) and NMR KCNQ1 VSD (PDB: 6MIE) (B) structures. Amino acid residues involved in the interaction between S1 and S4 segments as well as the charge transfer center (F167) and the fourth arginine (R237) of the S4 segment are depicted by stick models.

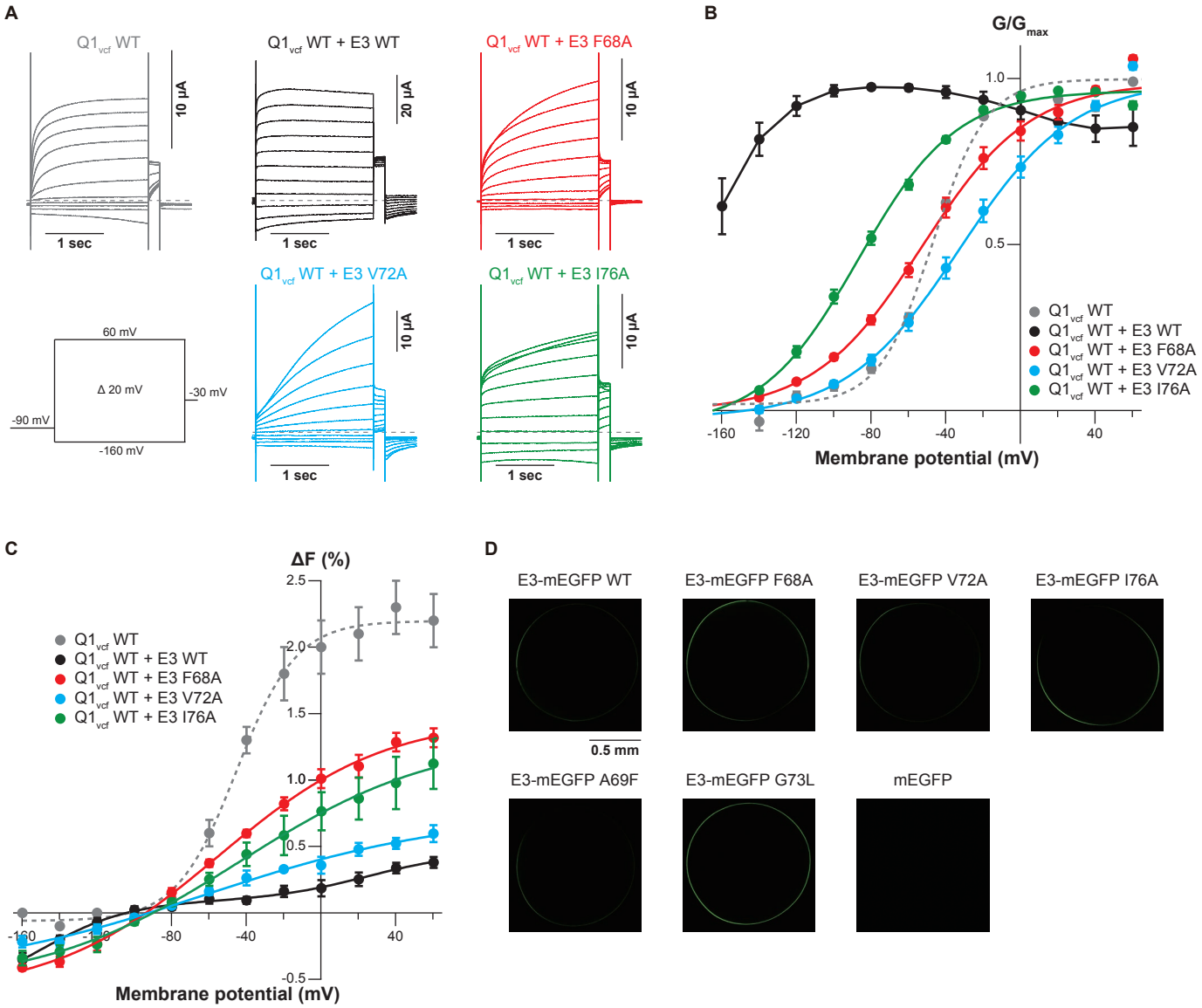


**Figure supplement 1, related to Figure 1. Current traces, G-V and F-V relationships of KCNQ1$_{vcf}$ WT and mutants, and the locatization of KCNE3 WT and mutants.**

(**A-C**) Representative current traces (A), G-V relationships (B), and F-V relationships (C) of KCNQ1$_{vcf}$ WT alone as well as KCNQ1 $_{vcf}$ WT in the presence of KCNE3 WT or one of the mutants. Error bars indicate ±s.e.m. for $n$ = 5 in (B, C). (**D**) Surface expression of the C-terminally mEGFP-tagged KCNE3 WT and all the KCNE3 mutants used in this study were confirmed by confocal microscopy. mEGFP without KCNE3 was not detected at the surface. All KCNE3 constructs and mEGFP were co-expressed with KCNQ1 WT.

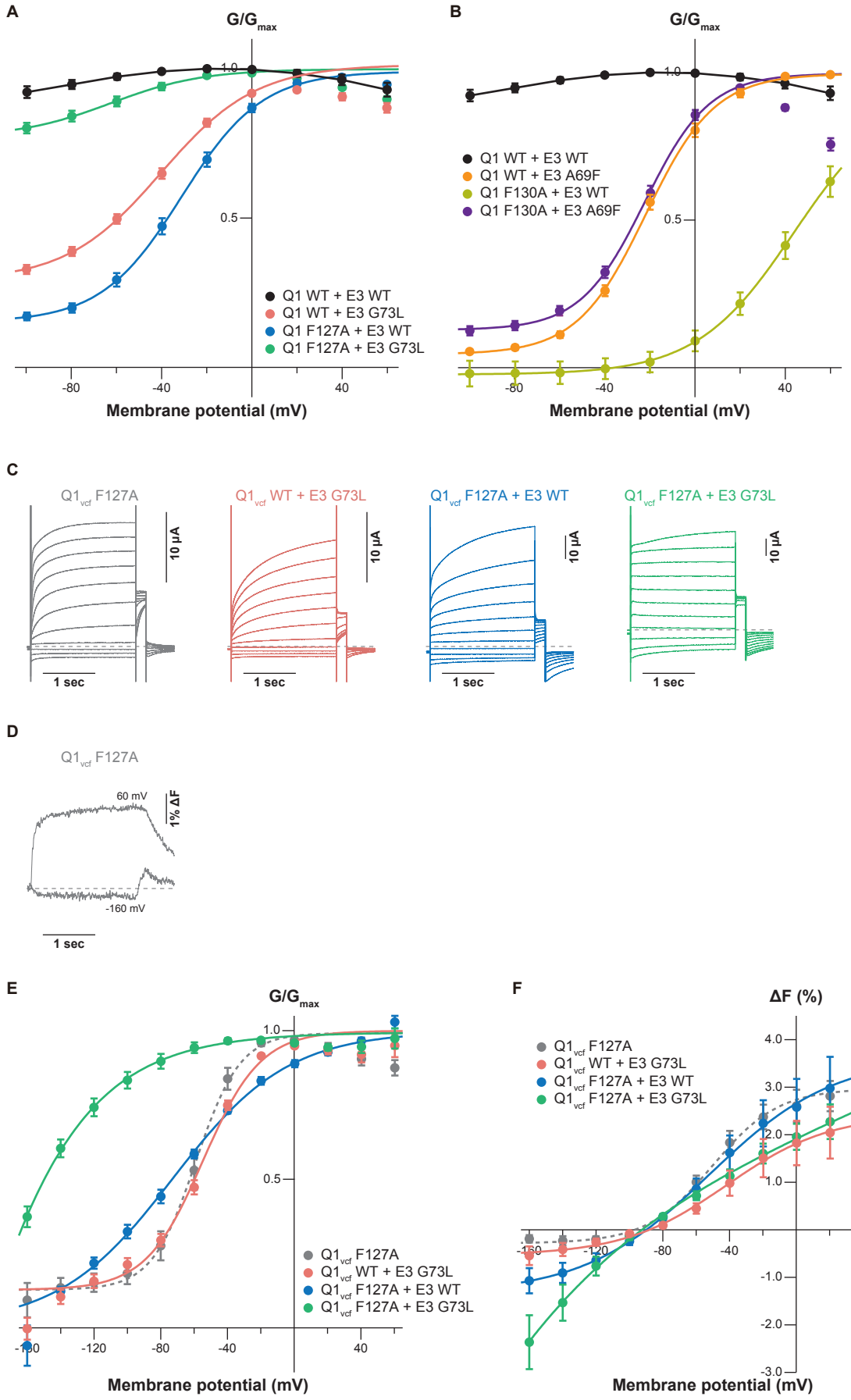
A
G/G$_{max}$
1.0
0.5
Q1 WT + E3 WT
Q1 WT + E3 G73L
Q1 F127A + E3 WT
Q1 F127A + E3 G73L
-80
-40
40
Membrane potential (mV)
B
G/G$_{max}$
1.0
0.5
Q1 WT + E3 WT
Q1 WT + E3 A69F
Q1 F130A + E3 WT
Q1 F130A + E3 A69F
-80
-40
40
Membrane potential (mV)
C
Q1$_{vcf}$ F127A
Q1$_{vcf}$ WT + E3 G73L
Q1$_{vcf}$ F127A + E3 WT
Q1$_{vcf}$ F127A + E3 G73L
10 µA
1 sec
D
Q1$_{vcf}$ F127A
60 mV
1% ΔF
-160 mV
1 sec
E
G/G$_{max}$
1.0
0.5
Q1$_{vcf}$ F127A
Q1$_{vcf}$ WT + E3 G73L
Q1$_{vcf}$ F127A + E3 WT
Q1$_{vcf}$ F127A + E3 G73L
-120
-80
-40
40
Membrane potential (mV)
F
ΔF (%)
Q1$_{vcf}$ F127A
Q1$_{vcf}$ WT + E3 G73L
Q1$_{vcf}$ F127A + E3 WT
Q1$_{vcf}$ F127A + E3 G73L
4.0
3.0
2.0
1.0
-1.0
-2.0
-3.0
-120
-80
-40
40
Membrane potential (mV)

**Figure supplement 2, related to Figure 3. Voltage-dependent kinetics of KCNQ1 S1 and $KCNQ1_{vcf}$ S1 mutants.**

(**A**) G-V relationships of KCNQ1 WT-KCNE3 WT, KCNQ1 WT-KCNE3 G73L, KCNQ1 F127A-KCNE3 WT, and KCNQ1 F127A-KCNE3 G73L. (**B**) G-V relationships of KCNQ1 WT-KCNE3 WT, KCNQ1 WT-KCNE3 A69F, KCNQ1 F130A-KCNE3 WT, and KCNQ1 F130A-KCNE3 A69F. (**C-F**) Representative current traces (C), fluorescence trace (D), G-V relationships (E), and F-V relationships (F) of $KCNQ1_{vcf}$ F127A, $KCNQ1_{vcf}$ WT-KCNE3 G73L, $KCNQ1_{vcf}$ F127A-KCNE3 WT, and $KCNQ1_{vcf}$ F127A-KCNE3 G73L. Error bars indicate ±s.e.m. for $n = 5$ in (A, B, E, F).

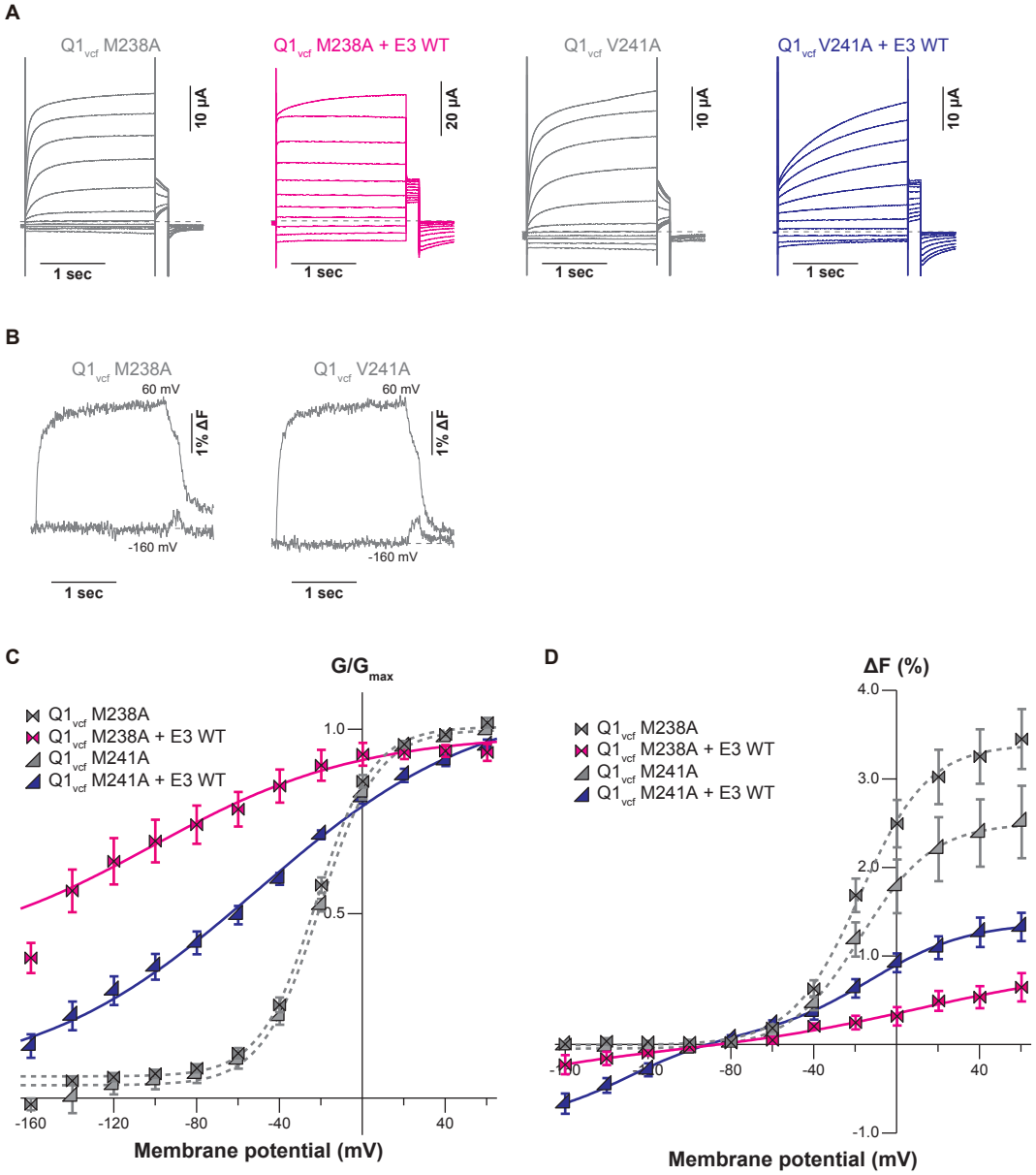


**Figure supplement 3, related to Figure 4. Voltage-dependent kinetics and KCNE3 effects of KCNQ1$_{vcf}$ S4 mutants.**

(**A, C, D**) Representative current traces (A), G-V relationships (C), and F-V relationships (D) of KCNQ1$_{vcf}$ M238A, KCNQ1$_{vcf}$ M238A-KCNE3 WT, KCNQ1$_{vcf}$ V241A, and KCNQ1$_{vcf}$ V241A-KCNE3 WT. Error bars indicate ±s.e.m. for $n$ = 5 in (C, D). (**B**) Fluorescence traces of KCNQ1$_{vcf}$ M238A and KCNQ1$_{vcf}$ V241A.

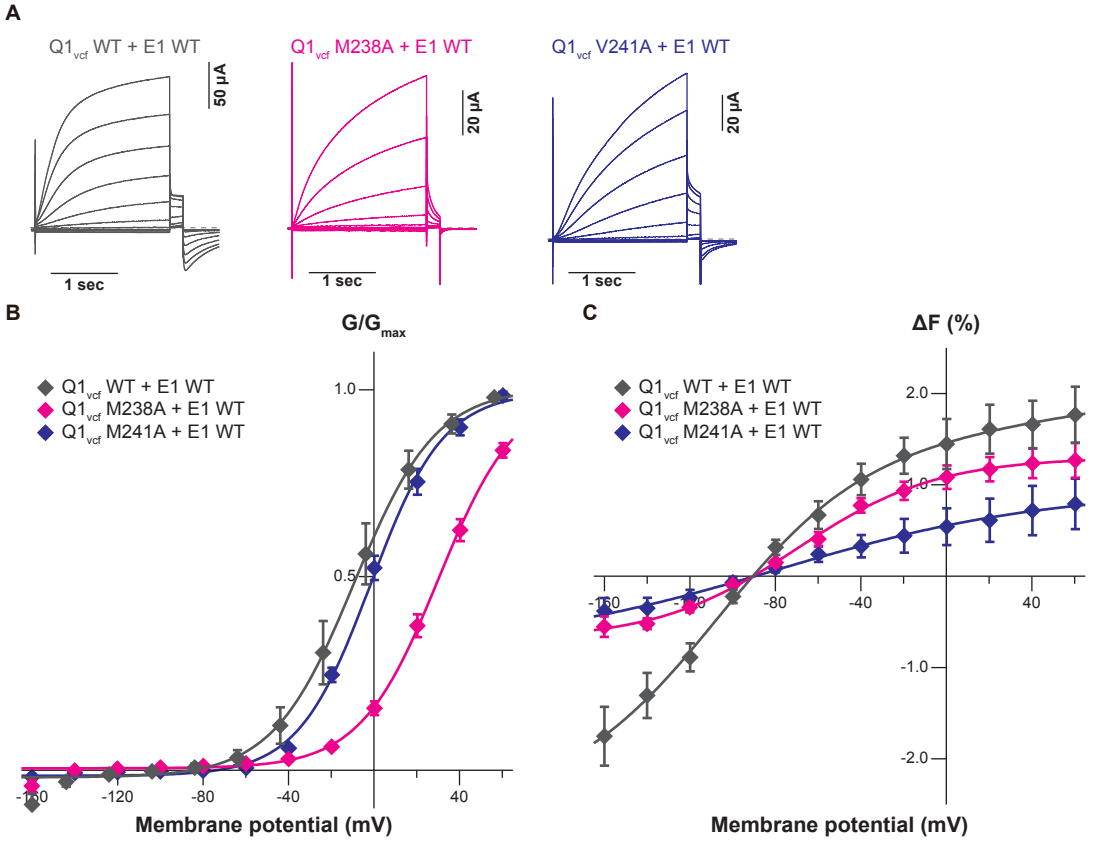


**Figure supplement 4, related to Figure 5. Voltage-dependent kinetics and KCNE1 effects of KCNQ1$_{vcf}$ S4 mutants.**

(**A-C**) Representative current traces (A), G-V relationships (B), and F-V relationships (C) of KCNQ1$_{vcf}$ WT-KCNE1 WT, KCNQ1$_{vcf}$ M238A-KCNE1 WT, and KCNQ1$_{vcf}$ V241A-KCNE1 WT. Error bars indicate ±s.e.m. for $n$ = 5 in (B, C).

| **Figure 1** | $G_{max}$ (µA) | $G_{-100}$ (µA) | $V_{1/2}$ (mV) | $z$ | $n$ |
|---|---|---|---|---|---|
| KCNQ1 WT | 2.2± 0.1 | 0.2 ± 0.0 | -22.9 ± 1.1 | 2.6 ± 0.1 | 5 |
| KCNQ1 WT + KCNE3 WT | 3.3 ± 0.5 | 2.8 ± 0.5 | n.d. | n.d. | 6 |
| KCNQ1 WT + KCNE3 F68A | 1.2 ± 0.1 | 0.2 ± 0.0 | -24.0 ± 1.4 | 1.4 ± 0.2 | 6 |
| KCNQ1 WT + KCNE3 V72A | 0.7 ± 0.4 | 0.0 ± 0.0 | -15.4 ± 6.4 | 0.8 ± 0.1 | 5 |
| KCNQ1 WT + KCNE3 I76A | 3.9 ± 1.0 | 0.2 ± 0.0 | -26.5 ± 1.5 | 1.6 ± 0.1 | 6 |
| **Figure 2** | | | | | |
| KCNQ1 F127A + KCNE3 WT | 0.7 ± 0.1 | 0.1 ± 0.0 | -36.1 ± 2.8 | 1.4 ± 0.0 | 5 |
| KCNQ1 F127A + KCNE3 F68A | 1.0 ± 0.0 | 0.2 ± 0.0 | -26.2 ± 0.8 | 2.0 ± 0.0 | 5 |
| KCNQ1 F127A + KCNE3 V72A | 0.6 ± 0.1 | 0.0 ± 0.0 | -33.5 ± 1.0 | 1.2 ± 0.0 | 5 |
| KCNQ1 F127A + KCNE3 I76A | 1.9 ± 0.4 | 0.1 ± 0.0 | +32.3 ± 5.0 | 0.8 ± 0.0 | 5 |
| KCNQ1 F130A + KCNE3 WT | 0.7 ± 0.2 | 0.0 ± 0.0 | +28.3 ± 2.3 | 1.2 ± 0.0 | 6 |
| KCNQ1 F130A + KCNE3 F68A | 0.4 ± 0.1 | 0.0 ± 0.0 | -18.3 ± 0.8 | 1.8 ± 0.1 | 6 |
| KCNQ1 F130A + KCNE3 V72A | 0.5 ± 0.2 | 0.0 ± 0.0 | +45.5 ± 1.7 | 1.3 ± 0.1 | 6 |
| KCNQ1 F130A + KCNE3 I76A | 0.2 ± 0.0 | 0.0 ± 0.0 | +6.1 ± 2.3 | 1.1 ± 0.0 | 6 |
| **Figure 3** | | | | | |
| KCNQ1 WT + KCNE3 WT | 5.4 ± 0.4 | 5.0 ± 0.4 | n.d. | n.d. | 10 |
| KCNQ1 WT + KCNE3 G73L | 2.8 ± 0.4 | 0.9 ± 0.1 | -40.1 ± 2.0 | 1.3 ± 0.0 | 9 |
| KCNQ1 F127A +KCNE3 WT | 1.5 ± 0.1 | 0.3 ± 0.0 | -30.1 ± 2.0 | 1.4 ± 0.0 | 10 |
| KCNQ1 F127A +KCNE3 G73L | 3.5 ± 0.3 | 2.8 ± 0.3 | n.d. | n.d. | 10 |
| KCNQ1 WT + KCNE3 A69F | 3.2 ± 0.5 | 0.2 ± 0.0 | -21.4 ± 1.5 | 1.7 ± 0.1 | 10 |
| KCNQ1 F130A +KCNE3 WT | 0.4 ± 0.1 | 0.0 ± 0.0 | +47.4 ± 3.4 | 1.2 ± 0.1 | 10 |
| KCNQ1 F130A +KCNE3 A69F | 0.6 ± 0.1 | 0.1 ± 0.0 | -22.1 ± 1.1 | 1.8 ± 0.1 | 10 |
| **Figure 4** | | | | | |
| KCNQ1 M238A | 0.8 ± 0.2 | 0.0 ± 0.0 | -1.7 ± 1.1 | 2.7 ± 0.1 | 10 |
| KCNQ1 M238A + KCNE3 WT | 1.0 ± 0.2 | 0.1 ± 0.0 | -42.3 ± 1.2 | 1.2 ± 0.0 | 10 |
| KCNQ1 V241A | 0.5 ± 0.1 | 0.0 ± 0.0 | -2.5 ± 0.9 | 2.3 ± 0.1 | 10 |
| KCNQ1 V241A+ KCNE3 WT | 0.8 ± 0.1 | 0.1 ± 0.0 | -39.0 ± 2.1 | 1.3 ± 0.0 | 8 |
| **Figure 5** | | | | | |
| KCNQ1 WT + KCNE1 WT | 13.1 ± 1.3 | 0.1 ± 0.0 | +39.4 ± 2.4 | 1.7 ± 0.1 | 6 |
| KCNQ1 M238A +KCNE1 WT | 12.3 ± 2.0 | 0.0 ± 0.0 | +23.9 ± 2.7 | 1.7 ± 0.0 | 10 |
| KCNQ1 V241A + KCNE1 WT | 7.1 ± 1.4 | 0.0 ± 0.0 | +50.2± 4.0 | 2.1 ± 0.1 | 9 |

**Table supplement 1, Summary of the constructs used in this study and their electrophysiological properties.** Maximum tail current amplitudes $G_{max}$, tail current amplitudes at -100 mV $G_{-100}$, and parameters deduced from the Boltzmann fitting ($V_{1/2}$ and $z$) for the KCNQ1/KCNE3 mutants. $n$ is the number of experiments. Same sample names appear in two lines (e.g. KCNQ1 WT + KCNE3 WT appears in Figure 1 and 3) because they are from different data sets.